Ultrasonics 117 (2021) 106556

Contents lists available at ScienceDirect

Ultrasonics

journal homepage: www.elsevier.com/locate/ultras

Fast and non-destructive ultrasonic test for face masks

Tomás E. Gómez Álvarez-Arenas [a,*], María D. Fariñas [b], Alba Ginel [a]

[a] Department of Ultrasonic and Sensors Technologies, Physical and Information Technologies Institute ITEFI, Spanish National Research Council (CSIC), Serrano 144, Madrid 28006, Spain

[b] Department of Food Technology, Universitat Politècnica de València, Camí de Vera, s/n, 46022 Valencia, Spain

ARTICLE INFO

Keywords:
Face masks
Non-destructive test
Air-coupled ultrasound

ABSTRACT

As a consequence of the large demand of face masks due to the COVID19 pandemic, cheap, fast and non-destructive tests that can verify in-line the variability of the filtration capacities, prove the potential disinfection and/or evaluate the performance of new filtering materials are needed. Using two different approaches based on air-coupled ultrasounds (0.15–1.6 MHz) with equivalent results, this work shows that each face mask presents a distinctive ultrasonic signature that enables the classification and the evaluation of their performance. Moreover, it is shown that the ultrasonic propagation through the face masks and the main filter layers takes place through the pore space and that low frequency response of the attenuation and the velocity is highly dispersive and is dominated by the interaction between the air in the pores and the fibers in the filters. Hence, the parameters that describe ultrasonic velocity, attenuation and dispersion can be related with their filtration efficiency and breathability. These techniques are fully contactless, non-invasive and fast.

1. Introduction

The global pandemic of coronavirus disease (COVID-19) that hit the world at the beginning of 2020 dramatically increased the demand of face masks [1]. These among other personal protective equipment (PPE), have been used as a physical barrier against the spreading of the virus whose transmission it is thought to rely fundamentally on three mechanisms: droplets, aerosols and contact [2]. Therefore, many countries took actions recommending hygiene, social distancing and the use of face masks in order to slow down the spread of the pandemic [3]. As consequence, the supply chain on these products was under high stress and during first stages of the COVID-19 pandemic, the market was not able to meet the demand. Then, for instance, the US Centers for Disease Control and Prevention (CDC) and the European Union, relaxed the existing standards, gave public guidance to use alternatives made of clothing fabric [4,5] and issued use guidelines intended to prevent shortage [6].

In the context of COVID-19, the following types of face masks are available according to World Health Organization (2020): (i) respirators or Face Filtering Piece (FFP), which protect the wearer from aerosols or particles that might be infectious or harmful on its surroundings (included as PPE); (ii) Medical Mouth-Nose Protection (MNP) or surgical masks, which are intended to protect others from exhaled potential harmful particles; (iii) masks for everyday use, which grant no protection for the user to be infected but it is assumed that provide a reduction of potential viral spread [7].

Face masks have to balance two main features: breathability and efficiency, while other important factors are: cost, time of use, and the possibility to reuse and disinfect them [8,9]. Regarding the efficacy of the face masks there are two main considerations: the performance of the material at filtering and the fitting of the design to the user [3]. Filtration is achieved by forcing the air to pass through a membrane that has the capability to retain the target particles or droplets. This membrane is made of a porous material with open porosity. Filtration efficiency depends on the type and the strength of the interaction between the solid material in the membrane and the particles to be retained in it (mechanical, electrostatic, chemical, biochemical, etc.) and on the factors that can enhance the possibility of this interaction. These factors depend on intrinsic pore properties as the porosity, the pore size, the pore tortuosity and sinuosity, the internal surface area and on other external factors as the thickness of the membrane and the use of several layers. Clearly, they also depend on the particles to be retained: size, shape, state (solid or fluid), concentration, electrostatic charge, etc. In some aspects, filtration efficiency and breathability can be opposite.

There are different standards to classify face masks efficacy: In the case of respirators, US National Institute for Occupational Safety and

* Corresponding author.
E-mail address: t.gomez@csic.es (T.E. Gómez Álvarez-Arenas).

https://doi.org/10.1016/j.ultras.2021.106556
Received 7 April 2021; Received in revised form 16 July 2021; Accepted 16 August 2021
Available online 19 August 2021

Health (NIOSH) established 9 categories (N95, N99, N100, P95, P99, P100, R95, R99, R100) taking into account whether they resist oil droplets (N, not resistant; R, somewhat resistant; P, strongly resistant) and their filtration efficiency (95, 99, 100%). The European Standard (EN 149:2001) classified the respirators into three main categories: FFP1, FFP2 and FFP3 regarding its minimum filtration efficiencies (80, 94, 99%). According to Lee et al., [10], other existing standards as the Chinese (KN95, GB2626-2006), the Korean (AS/NZ P2) and the Japanese (DS2 FFRs) were proven to be approximately equivalent to N95 and FFP2.

To assess the performance of the masks some features are tested such as filter penetration (NaCl aerosol at a determined flow rate -upstream/downstream- and particle size), flammability, extended exposure, breathing resistance and Total Inward Leakage (TIL) [11]. According to the American Society of Testing and Materials (ASTM) F2100 standard, (see, for example, [12]), five performance characteristics have been identified: particulate filtration efficiency (PFE), bacterial filtration efficiency (BFE), fluid resistance, differential pressure, and flammability. According to Chua et al. [12], the viral filtration efficiency (VFE) is another parameter used for certain N95 filtering respirators, although it is not currently recognized as a standard test method by ASTM. In this respect, it should be noted that even though the different certifications aforementioned are widely recognized, the test protocols employed are not completely similar. Furthermore, the final certification of the face masks for each territory must be achieved at an accredited laboratory. Also, some inconsistencies between face masks of different manufacturers certified by EN norms were reported by Serfozo, Ondráček, Zíková, Lazaridis, & Ždímal [13]. These procedures might become an issue when a rapid manufacturing response is needed as it was in 2020. In this sense, new, rapid and efficient testing methods that can give valuable information regarding filtering performance and guide along the mask selection process are needed, see for example Fischer et al., [14,13].

The breathability of the face masks is normally characterized by measuring the Maximum Breathing Resistance (MBR) for exhalation (at 30 and 95 l/min) and inhalation (at 160 l/min) or the Differential Pressure (previously mentioned), that measures the ability of the mask material to restrict airflow through it, giving an objective indication of the mask's breathability.

The large demands of face masks in the wake of the worsening and prolonging COVID-19 pandemic, raises some other issues (see Chua et al. [12]), like the use of masks made of household materials, the use of decontamination methods [8,9], the research in new filtration materials and some environmental issues related to the consumption of natural resources and disposable of waste material. Recently, professionals from different fields where the use of PPE has dramatically increased during the pandemic are raising their voices about the upcoming sustainability and environmental issues that this might represent and claim for further research towards the impact mitigation of those (see for example, [15]). In this context, there is also a demand of scientific advice on the reuse of face masks in the private environment (see, [16]).

Together with the necessity to determine the filtration capability, breathability and durability of the selected materials according to the approved standards, there is also a demand to develop cheap, fast and non-destructive tests that can, among others activities: (i) verify in-line that the variability of the produced filtration material is within the acceptable tolerance, (ii) verify face mask integrity after disinfection [8,9], (iii) test the performance of new filtering materials and membranes, (iv) optimize the use of materials to reduce waste [8,16].

Ultrasonic methods have been previously used to study, test and characterize filtration membranes [17–21]. A general formulation of the wave propagation problem in fluid-saturated porous materials was produced by M.A. Biot (see [22,23]), with the main assumptions of open porosity and wavelength larger than typical pore size. In general, this formulation predicts the propagation of two longitudinal waves (first and second types or fast and slow longitudinal modes). Under some approximations, these modes can be understood as fluid-borne and a structure-borne propagation modes. The observability of these two modes depends on the possibility to generate them (which depends on boundary conditions), on the attenuation coefficient and the propagation length. Biot distinguished between two different frequency regimes. In the low frequency range, viscous skin depth is larger than the pore size and the wave propagation in the fluid is dominated by this interaction between the fluid and the pore walls. In this case, the fluid-borne propagation is strongly dispersive with velocity and attenuation coefficient varying with the frequency (f) as: $f^{0.5}$. In the high frequency range, the fluid-borne propagation is mostly free of this viscous friction and the propagation is mainly affected by pore space geometry (tortuosity).

A well-known example in this context is the study of sound propagation in fibrous-porous materials saturated by air as these materials are widely used as acoustical absorbers (see, for example [24,25]). In these cases, only the fluid-borne propagation is observed and the low frequency limit is many times valid. In such cases, Biot's formulation is reduced to the "modified fluid approach". Ultrasonic propagation in air-saturated fabrics was studied in Álvarez-Arenas [26]. This work demonstrates that in this case, only the fluid-borne propagation is observed. Other examples of the use of ultrasonic techniques to the study of air-saturated membranes and filters correspond to Álvarez-Arenas et al. [19,27], where only the solid-borne wave was observed and ion-track membranes, where both wave types were observed, and the role of the surface porosity in the possibility to generate the fluid-borne propagation mode was investigated (see, [28,29]). These works show the potential of this technique as an alternative for non-invasive characterization of filters or even as an integrity test in the light of the high correlations obtained against membrane properties such as porosity, permeability, pore size and other filtration parameters. In the context of face mask characterization, it is then clear that the measurement of the ultrasonic propagation in the face mask have the potential to provide information about both filtration efficiency and breathability.

In this work, we report the results of the study of the propagation of ultrasonic waves (in air) through face masks and face mask component layers with the purpose to determine the possibilities of this approach to characterize or test these materials. The studied frequency range is 0.15–1.6 MHz and two different techniques were employed. We have measured transmission coefficient spectra (magnitude and phase) and analyzed the results to obtain some parameters like attenuation coefficient, ultrasonic velocity and dispersion. The correlation between ultrasonic parameters and other face mask properties is discussed as well as the possibilities to develop and use a fast and simple ultrasonic test for in-line quality control in face mask fabrication or as a rapid test to study modifications of face masks with the use or after being treated.

2. Materials and methods

2.1. Face masks

We tested 9 different face masks of different type and from different manufacturers. Face masks description and available information is listed in Table 1,. With the exception of reusable face masks, made of fabric, in general, face masks are made of two external and very thin layers and between then one to three inner layers. One significant difference observed between the reusable fabric face masks and the rest of the face masks studied here is that fabric face masks are stretchable. Therefore, it can be anticipated that any stretching (either in use or during testing) can affect the face mask properties and efficiency. In this case all face masks were tested without any stretching. In general (see for instance, [12]), the outermost layer is waterproof and helps to repel fluids and droplets. The inner layers (one or more) are the filter layers, which prevents particles or pathogens above a certain size from penetrating in either direction. The innermost layer is similar to the outermost one and is made of absorbent materials to trap droplets and to

Table 1
Description of the face mask used in this study and information obtained from manufacturers.

Name	Description	Other data
Hygienic	UNE 0064–1:2020 Three layers : woven PP / blown PP / woven PP	By Asia Biomed Technology
Hygienic, reusable	One layer, fabric, UNE 0065/20 y OEKO-TEX 100	By Abbacino
Fabric	Two layers	n.a.
Surgical	Three layers	n.a
KN95 PinzTech	Three layers Standard GB2626-2006, NK95	By Xiamen PinzTech
FFP2 Aura	FFP2 –NR, four layers, EN149:2001, CE2797 Maximum breathing resistance: Inhalation 30 l/min: 0.7 mbar Inhalation 95 l/min: 2.4 mbar Exhalation 160 l/min: 3.0 mbar	Aura™ 9320+, by 3 M*
FFP2 Biofield	FFP2 –NR, four layers, EN149:2001 + A1:2009 CE2163, filtration efficiency > 94%	Biofield, by Zhejiang Lily
FFP2 Palens	FFP2, three layers PP/PP/nanofiber layer (external), EN 149: 2001 + A1: 2009, COVID-19. CE 0370–4080-PPE/B Mean filtration efficiency: 96,4% Maximum breathing resistance: Inhalation 30 l/min: 0,37 mbar Inhalation 95 l/min: 1.54 mbar Exhalation 160 l/min: 2.2 mbar	Palens PLNS1619 by Bioinicia†
FFP3 Sicura	FFP3, Five layers, EN149: 2001 + A1: 2009 Filtration efficiency > 99%	Sicura P30 by Metalsud lo gatto

* Technical data sheet available in: https://multimedia.3 m.com/mws/media/842338O/aura-9300-series-respiratory-technical-datasheet-pdf.pdf
† Further information in: https://bioinicia.com/comunicado-sobre-la-mascara-filtrante-palens-plns1619/

absorb the moisture from exhaled air to contribute to improve the user comfort and the face mask durability.

External layers are, normally, membranes made of blown polypropylene and the main function is to protect the filter layers located between them and avoid direct contact between the filter layer and the mouth. Inner layers are, normally, made of non-woven fibers. The different layers in the face masks can be easily separated.

Surgical masks and FFP respirators can be differentiated by the time of use (<4 h and < 8 h, respectively) and by the filtering efficiency: FFP2 masks, filtering ≥ 94% of aerosols (total inward leakage < 8%) and FFP3 masks, filtering ≥ 99% of aerosols (total inward leakage < 2%) [6].

2.2. Ultrasonic measurements

All measurements were performed in the ITEFI-CSIC during December 2020 at constant conditions of temperature (25 °C) and humidity (35%). All measurements were taken in a short period of time after removing the face mask from their envelope. It can be anticipated that temperature will affect in some extent to the measured ultrasonic response, while the presence of humidity trapped in the face mask can modify the face mask properties so we have avoided these effects by keeping temperature constant and humidity constant and as low as possible.

2.2.1. Wideband ultrasonic measurements

Three pairs of ultrasonic transducers specifically optimized for its use in air with centre working frequencies of 0.25, 0.65 and 1.1 MHz were employed [30]. These transducers were designed and fabricated by our group and are intended to optimize both sensitivity and bandwidth simultaneously for ultrasonic air-coupled operation. Usable frequency range is 0.15–0.35 MHz, 0.3–0.9 MHz and 0.6–1.6 MHz, for the 0.25, 0.65 and 1.1 MHz transducers, respectively. Therefore, it is possible to combine these three pairs to obtain measurements in the frequency range 0.15–1.6 MHz. All measurements in the face masks and the component layers were taken in through transmission configuration: the transducers were placed facing each other while the sample under test was located in between, assuring normal incidence of the ultrasonic wave. Both face masks and layer components are placed flat on this cavitiy avoiding any stretching, especially in the case of reusable stretchable fabric face masks For these measurements, transducers mounted on U-shaped holders, previously used and described (see, for example, [31]) were used, transducers were fixed and a slot is provided to introduce the sample, this facilitates the measurements. A picture of the devices with the face masks is shown in Supp. Mat.

A commercial pulser-receiver (5077PR, Olympus, Houston, TX, USA) was used to drive a 200 V-semicycle-square-wave tuned at the corresponding central frequency of the transmitter. The received signal was amplified (20 dB), averaged (12 samples) and digitalized at 10 MS/s using a commercial digital oscilloscope (7054, Tektronix, WA, USA). Then, magnitude and phase spectra of the transmitted signal were calculated. Prior to every test, a blank measurement was taken in order to compute the transmission coefficient spectra, following the same procedure as in [29]. Three different face masks for each type listed in Table 1 were used, and each one of them was measured in two or three different points. With the exception of reusable face masks where there was only one sample available and they were measured at five different

Table 2
Thickness and density of face masks and their component layers.

Facemask	Thickness (μm)	Density (kg/m^3)
Hygienic		
Whole facemask	360 ± 30	220 ± 30
External layer (outwards)	125 ± 15	215 ± 30
Filter layer	120 ± 15	230 ± 25
External layer (inwards)	120 ± 15	225 ± 30
Hygienic, reusable		
Whole facemask	585 ± 40	345 ± 30
Reusable		
Whole facemask	520 ± 40	335 ± 30
Surgical		
Whole facemask	370 ± 40	210 ± 40
External layer (outwards)	130 ± 20	200 ± 50
Filter layer	115 ± 20	250 ± 55
External layer (inwards)	130 ± 15	200 ± 40
KN95 PinzTech		
Whole facemask	735 ± 60	230 ± 30
External layer (outwards)	240 ± 20	220 ± 30
Filter layer	255 ± 30	235 ± 50
External layer (inwards)	230 ± 15	230 ± 30
FFP2 Palens		
Whole facemask	660 ± 60	215 ± 40
External layer (outwards)	190 ± 15	205 ± 25
Filter layer	275 ± 15	230 ± 20
External layer (inwards)	195 ± 25	200 ± 55
FFP2 Aura		
Whole facemask	1200 ± 100	265 ± 50
External layer (outwards)	205 ± 35	220 ± 60
Filter layer	490 ± 20	215 ± 15
Additional filter layer	371 ± 50	365 ± 110
External layer (inwards)	120 ± 15	240 ± 30
FFP2 Biofield		
Whole facemask	780 ± 60	230 ± 35
External layer (outwards)	220 ± 25	230 ± 50
Filter layer	190 ± 20	280 ± 20
Additional filter layer	205 ± 20	205 ± 15
External layer (inwards)	170 ± 15	220 ± 25
FFP3 Sicura		
Whole facemask	830 ± 45	311 ± 36
External layer (outwards)	220 ± 10	298 ± 20
Filter layer	154 ± 10	322 ± 35
Additional filter layer	187 ± 10	325 ± 30
Additional filter layer	142 ± 10	360 ± 30
External layer (inwards)	124 ± 10	245 ± 75

locations. The different measurements obtained for every type of sample were averaged and standard deviation calculated. Finally, and for the purpose of a clearer display of the measurements in the figures, all measured spectra were resampled at a lower frequency to reduce the number of points in the figures.

2.2.2. Narrowband measurements

The two pair of air-coupled ultrasonic transducers whose center frequencies is 0.25 and 1.1 MHz were used for these measurements. They were excited with a sine tone burst of 15 cycles with 20 V amplitude using a commercial function generator (Agilent 330A; Santa Clara, USA). A reference signal was acquired to every measurement. In all cases, the received signal was averaged, digitalized and stored by using a commercial digital oscilloscope (5072, Tektronix, WA, USA). Selected frequencies for these measurements were 0.3, 0.7 and 1.4 MHz. For the 0.3 MHz frequency, the transducers centered at 0.25 MHz were used while for the measurements at 0.7 and 1.4 MHz, the pair at 1.1 MHz were used. The same U-shaped holders were used in this case. The amplitude ratio of the measurement to the reference signal was used to compute the transmission coefficient magnitude, while the phase shift between measurement and reference signal was employed to calculate the phase of the transmission coefficient. The results are shown in Table 4. These values were then compared with those obtained using the wide band signals and the spectrum analysis (Fig. 1).

2.3. Thickness and density

A micrometer (±0.01 mm; Mitutoyo, Kawasaki, Japan) was used to measure the thickness of the face masks studied as well as the thickness of every layer within them. Thickness was measured at four different points of each face mask, the mean value and the standard deviation was then computed. Additionally, density of the samples were calculated using excised circles (40 mm diameter, obtained using a punch holder), that were weighed in a precision balanced (XT 220A; Precisa Gravimetrics AG, Dietikon, Switzerland).

2.4. Microscopic images

A Leica DM750 (Leica Mycrosystems, Wetzlar, Germany) transmission microscope fitted with a Leica ICC50 HP camera were used. All images were obtained at x10/0.22. The LEICA DM750 microscope is fitted with an Abbe condenser whose aperture was used to optimize image brightness and contrast and to avoid light saturation. The larger the layer opacity of the sample, the larger the Abbe condenser aperture used. It was changed from x4 (typically for external membranes), up to x48 for some of the FFP2 filters.

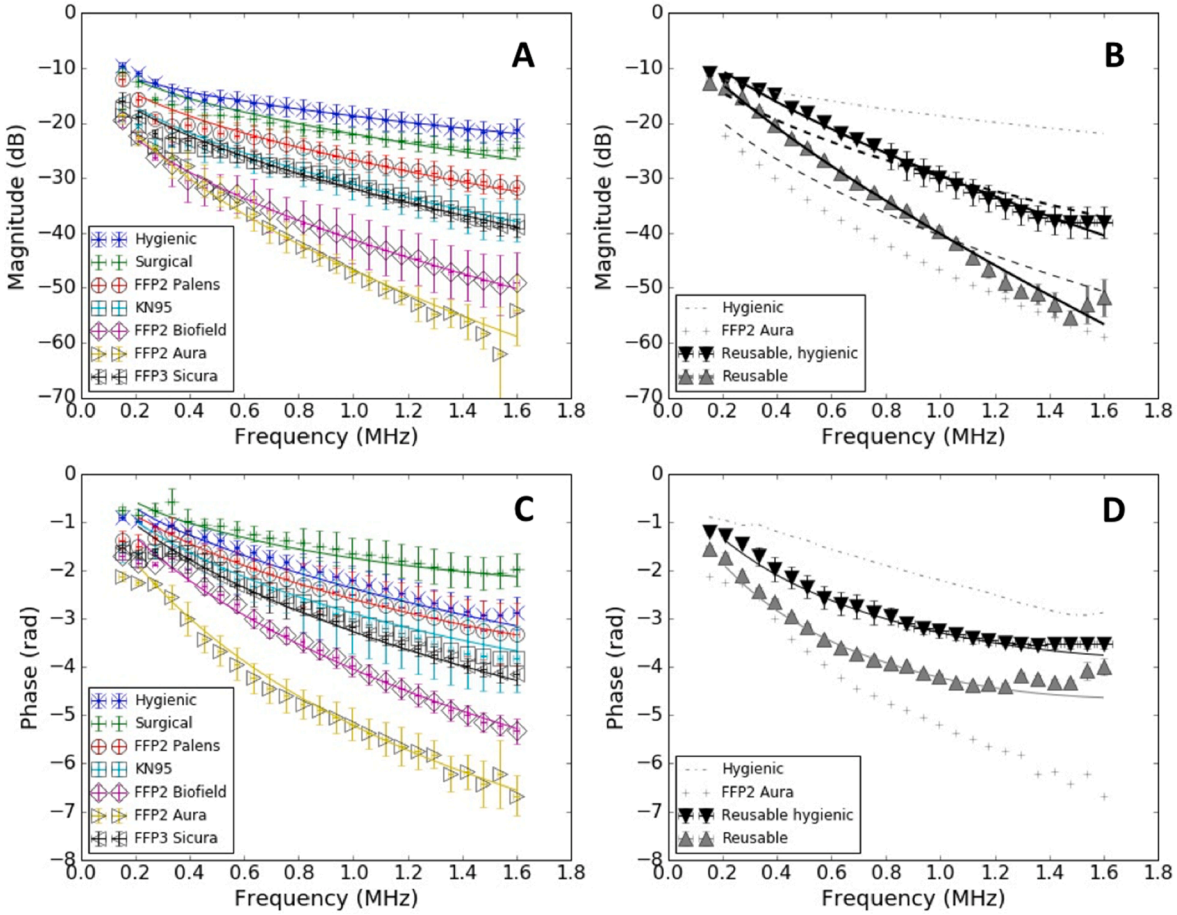

Fig. 1. Air-coupled ultrasonic transmission coefficient spectra for the whole face masks: (**A**) magnitude and (**C**) phase of the transmission coefficient vs frequency of non-reusable face masks. (**B**) magnitude and (**D**) phase of the transmission coefficient of reusable face masks: the upper and lower limits shown (gray symbols '+' and dash dotted line) correspond to the upper and lower limit observed in non-reusable face mask (that is: hygienic or surgical and FFP2 Aura) to make comparison easier. Solid lines correspond to the calculated transmission coefficient using Eqs. (1), (2), (6), and (7), with $n = 0.5$ (Eq. (7)), that correspond to the low-frequency Biot's poroelastic losses. Only for the reusable face masks (**B**) this approach ($n = 0.5$) shows a very poor fitting (dashed gray lines). In this case, the n factor is allowed to change to find the best fitting (solid line, **B**). The parameters obtained from the fitting of phase and magnitude spectra are in Table 2.

3. Results

3.1. Thickness and density measurements: Whole facemasks and component layers

As a preliminary and basic characterization of the face masks, both thickness and density of the whole face masks and their component layers were measured. Table 2 summarizes the results. The errors in Table 2 reflect both the variability of the measurement within one sample and within different samples from different face masks of the same type.

3.2. Wideband ultrasonic measurements

3.2.1. Whole facemask results

Fig. 1 shows the measured ultrasonic transmission coefficient spectra, magnitude and phase, for the whole face masks. A similar trend is observed for all face masks with the exception of the face masks made of woven textile (reusable and hygienic reusable), whose results are plotted separately for more clarity (Fig. 1B and 1D).

These measurements reveal four fundamental results: i) it is possible to measure the ultrasonic transmission coefficient spectra for the all the face masks using air-coupled ultrasound in the frequency range 0.15 – 1.6 MHz and the equipment described in the Materials and Methods section; ii) there is a clear difference in both the magnitude and the phase of the transmission coefficient spectra for the different face masks tested. In particular, with the face mask type and with the thickness and the density of the face masks (see Suppl. Mat. Section I, Fig. 1); iii) there is no evidence of ultrasound reverberations within the face masks (like results presented in [21,26,28,29,32]), these reverberations would give rise to thickness resonances that are not present here (as observed in other filtration membranes see [19,27]); iv) the observed ultrasonic transmission through the face masks correspond to the Biot's slow wave (as observed before in air-saturated ceramics and rocks [33], open cell foams with large pores [34,35], fabrics [26] and ion track membranes with pore size > 500 nm [21,28,29,32]), or second compressional wave that is, mainly, a fluid-borne propagation mode. This later result is relevant for this work as this implies that the transmitted ultrasonic wave through the face masks have the potential to provide information about the pore space: pore size, porosity, pore tortuosity, permeability, etc. that will be clearly related with face masks filtration efficiency and breathability (as discussed in [19,21,27,29,32,34,35]). This later result requires of a better explanation that is provided below.

Given the experimental set-up, and the fact that there are no thickness resonances, the effective ultrasound velocity of the propagation across the face masks is obtained directly from the phase spectrum measurement ($\Delta\phi$), the face mask thickness, t, and the velocity of ultrasound in the outer medium (air: $v_a = 340$ m/s) [36]:

$$v_s = \frac{t}{\Delta\phi/\omega + t/v_a} \tag{1}$$

Some examples of the variation in the ultrasonic velocity with the frequency obtained from measurements in Fig. 1 and Eq.1 are shown in Fig. S2. Obtained velocity shows a strong dispersive behavior at low frequency (velocity goes to zero as frequency goes to zero) and a rather constant value at high frequency. It is interesting that we can use this velocity data to verify that there are no thickness resonances in the face masks. Thickness resonances for through transmission and normal incidence appear at frequencies ($f_{res}(n)$) given by: $f_{res}(n) = v / (2t) \times n$, where n is the order of the resonance, $n = 1,2,3\ldots$ For example, for the hygienic face mask, $f_{res}(n = 1)$ is expected at 330 kHz, while for KN95 PinzTech $f_{res}(n = 1)$ is expected at 185 kHz. These frequencies are within the experimental range, however, no resonances are observed. This can be explained by a large attenuation coefficient, or a significant surface roughness and/or thickness variability.

The variation in the measured ultrasonic velocity with the frequency in the frequency range < 400 kHz can be described by Eq. (2.a) (see Suppl. Mat. Section II), that coincides with the variation in the velocity of the slow wave mode in the low frequency limit of the Biot's theory (2.b):

$$v \propto f^{0.5} \tag{2.a}$$

$$\frac{v}{v_c} = \left(2\frac{f}{f_c}\frac{(\sigma_{11}\sigma_{22} - \sigma_{12}^2)}{(\gamma_{11} + \gamma_{22})}\right)^{1/2} \tag{2.b}$$

where, σ_{ij} are the Biot's normalized elastic modulus for the solid (ij = 11), the fluid (ij = 22) and for the mechanical coupling between them (ij = 12), γ_{ij} are normalized densities for the solid (ij = 11), the fluid (ij = 22) and the inertial coupling between them (ij = 12), v_c a reference velocity and f_c is a reference frequency given by: $(\mu\phi^2/k)/(2\pi\rho_{fluid})$ where μ is the fluid viscosity, ϕ is the porosity, k is the permeability and $\rho_{fluid}$is the density of the fluid.

However, for frequencies over 400 kHz, this approach is no longer valid and the velocity approaches a constant value as it is also predicted in the Biot's high frequency limit, where velocity is given by:

$$v = \frac{v_{air}}{\sqrt{\tau}} \tag{3}$$

where τ is the pore tortuosity.

In the transition from the low to the high frequency limits, the variation in the velocity with the frequency can be represented by a general power law:

$$v \propto f^m \tag{4}$$

with $0 < m < 0.5$. This variation in the velocity with the frequency suggests that the observed propagation corresponds to the Biot's slow wave or second compressional wave or slow wave that is mainly related to the wave traveling through the air in the pores. Stronger evidence that supports this hypothesis can be obtained from the analysis of the magnitude of the transmission coefficient (Fig. 1). According to Biot's theory for the propagation of acoustic waves in fluid saturated porous media, transmission coefficient through the face mask, considering it as a slab of porous material, under normal incidence can be described as:

$$T = \phi T^f + (1 - \phi)T^s \tag{5}$$

where T^s and T^f are the solid-borne (fast wave) and fluid-borne (slow-wave) contributions and ϕ is a factor that takes into account the mode conversion phenomena at the surface of the porous material [37]. As made by Nagy [33], a simple estimation of the relative contribution of each propagation mode to the transmission coefficient can be obtained by the calculation of the loss due of the reflections at the face mask/air interfaces. The reflection coefficient (R) at the interface between two media (*1* and *2*) is given by: $R = ((Z_2 - Z_1) / (Z_2 + Z_1))^2$. Where Z is the acoustic impedance and subindexes *1* and *2* stand for the two media. We know that mean ultrasound velocity in the face masks is about 240–275 m/s (see Table 2 and Fig. S2). As the solid phase is mainly made of polypropylene (density = 1100 kg/m^3), and the fluid in the pores is air (density = 1.2 kg/m^3), then if the observed propagation (v ≈ 240–275 m/s) corresponds to the fast longitudinal, or solid-borne propagation mode, the acoustic impedance for this mode would be about 0.3 MRayl. On the contrary, if the observed propagation corresponds to the slow longitudinal mode, or pore-borne propagation, the acoustic impedance would be about 330 Rayl. As the acoustic impedance of the air is 408 Rayl, we can calculate the expected reflection coefficient for both modes: 0.9945 and 0.011 for the solid-borne and the fluid-borne propagation, respectively. That is, the expected loss in the transmission coefficient due to the reflection at the surfaces of the faces masks is about −45 dB and −0.1 dB for the solid-borne and the fluid borne propagation modes, respectively. Therefore, no contribution of the solid borne propagation mode above −45 dB is expected, and as already explained by Nagy [33], the large impedance mismatch between the fast-wave

impedance and the air, is the responsible for the poor or negligible generation of this mode. It must be underlined the fact that this simple analysis only considers the energy loss due to the reflection at the surface of the face masks and the contribution of the attenuation in the face mask is neglected. Therefore, any effect of the attenuation will push further down this contribution of the solid borne propagation. Given the observed values of the transmission coefficient magnitude loss (see Fig. 1) it is then clear that the contribution of this mode can be considered negligible. Moreover, given the reduced loss of the fluid borne propagation mode due to reflection at face mask/air interfaces (0.1 dB), this means that practically all the observed loss in Fig. 1 is due to the attenuation in the material. Therefore, a large attenuation coefficient in the material is expected. This large attenuation coefficient and the almost perfect impedance match between the slow-wave and the surrounding air are consistent with the fact that no thickness resonances are observed.

Therefore, we can assume that:

$$T = \phi T^f \tag{6}$$

where T^f, for a flat layer, normal incidence and uni-modal propagation is given by (see [38]):

$$T^f = 2/(2coskt + i(m + 1/m)sinkt) \tag{7}$$

where m is the ratio of the impedances of the layer to the air, t the layer thickness and k the complex wave vector: $k(\omega) = \omega/v(\omega) + i\alpha(\omega)$, where α is the attenuation coefficient, v the phase velocity and ω the angular frequency. Clearly, face masks are made of several layers with different properties and the transition from one layer to the next must affect the propagation of ultrasonic waves, nonetheless this first approach (considering the face mask as a homogeneous material) can be useful to quantify some effective properties of the whole face mask. A more detailed analysis of the individual layers is presented in next section.

Solid lines in the phase spectra (Fig. 1B) correspond to the calculated phase spectra (using Eqs. (6) and (7)) with a velocity given by:

$$v = v_0\left(\frac{f}{f_0}\right)^m \begin{cases} for f < 400kHz : f_0 = 200KHz, m = 0.5 \\ for f > 400kHz : f_0 = 1MHz \end{cases} \tag{8}$$

where fitting parameters are v_0 and m. Solid lines in the magnitude spectra (Fig. 1A) correspond to the calculated spectra (Eqs. (6) and (7)) using the velocity obtained before and an attenuation coefficient given by Eq. (9.a) where n is set equal to 0.5 as predicted by the Biot's low frequency limit Eq. (9.b):

$$\alpha = \alpha_0\left(\frac{f}{f_0}\right)^n \tag{9.a}$$

$$\frac{\alpha}{\alpha_c} = \left(\frac{1}{2}\frac{f}{f_c}\frac{(\gamma_{11} + \gamma_{22})}{(\sigma_{11}\sigma_{22} - \sigma_{12}^2)}\right)^{1/2} \tag{9.b}$$

The fitting parameters in this case are: ϕ in Eq. (6) (that can be approximated to the surface porosity [28,29,39] and α_0. The obtained fitting is quite good (see Fig. 1A). The exceptions are the woven face masks where a larger value of n is required to achieve a similar fitting quality. Fig. 1B shows the obtained fitting for the woven face masks using $n = 0.5$ (dashed line) and the obtained fitting using n as fitting parameter (solid line). All the obtained parameters from the analysis of the measurements in Fig. 1 are show in Table 3 .

3.2.2. Component layers results

The transmission coefficient spectra, magnitude and phase, for each layer component were also measured using the same technique as in previous section. Results are shown in Figs. 2 and 3. The filter layers (Fig. 2 and Fig. 3A and 3B) were analyzed as we did in the previous section. In the first place, velocity is described by Eq. (8), where v_0 and m are used as a fitting parameter to match phase spectrum calculation to

Table 3
Obtained parameters from the analysis of the ultrasonic transmission coefficient measurements.

Facemask	α_0 (Np/mm) $f_0 = 1$ MHz	n*	ϕ (Surface porosity)	v_0 (m/s) @ 1 MHz	m
Hygienic					
Whole	3263.9	0.5	0.48	250	0.1
facemask	11421.6	0.5	0.74	230	0.22
Filter					
Hygienic reusable	3703.7	0.67	0.85	260	0.15
Whole facemask					
Reusable					
Whole facemask	5791.7	0.74	0.85	235	0.22
Surgical					
Whole	4698.3	0.5	0.61	270	0.11
facemask	12467.1	0.5	0.73	225	0.25
Filter					
FFP2 Palens					
Whole	2472.1	0.5	0.57	280	0.076
facemask	2586.8	0.5	0.40	280	0.05
Filter					
KN95 PinzTech					
Whole	2468.8	0.5	0.53	280	0.08
facemask	5977.2	0.5	0.63	245	0.16
Filter					
FFP2 Biofield					
Whole	2888.2	0.5	0.41	265	0.09
facemask	11426.1	0.5	0.59	210	0.24
Filter	1502.4	1.32	0.84	305	0.02
Additional filter					
FFP2 Aura					
Whole	2084.3	0.5	0.85	275	0.09
facemask	3294.3	0.5	0.72	265	0.1
Filter	2862.1	0.98	1.0	285	0.16
Additional filter					
FFP3 Sicura					
Whole	2109.838	0.5	0.51	280	0.07
facemask	8189.404	0.5	0.56	210	0.1
Filter	1242.572	1.36	0.88	295	0.02
Additional filter	2231.059	1.37	0.88	295	0.02
Additional filter					

*: n values of 0.5 indicate that this parameter was fixed and not used as fitting parameter.

Table 4
Transmission coefficient magnitude and phase measured at 0.3, 0.7 and 1.4 MHz using a 15 cycles sinusoidal tone burst.

Facemask	Transmission coefficient					
	Magnitude (dB)			Phase (rad)		
	0.3 MHz (±2 dB)	0.7 MHz (±2 dB)	1.4 MHz (±4 dB)	0.3 MHz (±0.1 rad)	0.7 MHz (±0.1 rad)	1.4 MHz (±0.2 rad)
Hygienic	−13.6	−16.1	−21.3	−1.04	−1.5	−3.5
Surgical	−17.9	−18.6	−23.8	−1.04	−1.4	−2.6
KN95 PinzTech	−26	−28.5	−37.39	−2.83	−2.9	−4.6
FFP2 Palens	−17.2	−22.1	−27.7	−1.41	−2.0	−3.1
FFP2 Aura	−24.3	−37.9	−55.0	−1.98	−4.5	−6.2
FFP2 Biofield	−28.7	−33.6	−44.4	−1.41	−2.86	−5.3
FFP3 Sicura P30	−22.3	−28.5	−38.7	−1.75	−2.73	−5.63

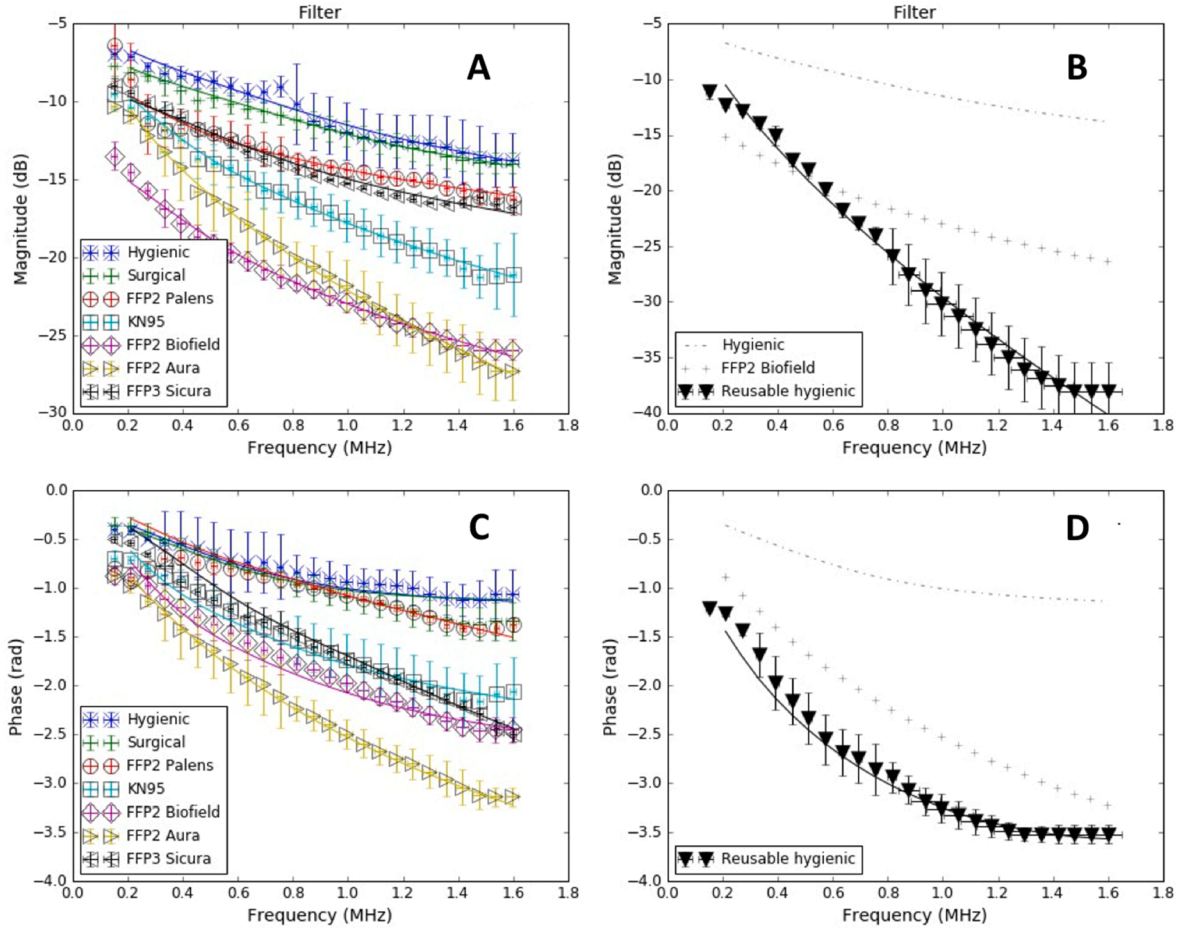

Fig. 2. Air-coupled ultrasonic transmission coefficient spectra for the main filter layer of the face masks: (**A**) magnitude and (**C**) phase of the transmission coefficient vs frequency of non-reusable face masks. (**B**) magnitude and (**D**) phase of the transmission coefficient of reusable face masks. Since reusable face mask has no filter layer, the result here correspond to the whole face mask (single layer) and it is shown for comparison purposes. In (**B**) and (**D**), the upper and lower limits shown (gray symbols '+' and dash dotted line) correspond to the upper and lower limit observed in non-reusable face mask (that is: hygienic and FFP2 Aura or Biofield) to make comparison easier. Solid lines correspond to the calculated transmission coefficient using Eqs. (1), 2, 6, and 7, with $n = 0.5$ (Eq. (7)), that correspond to the low-frequency Biot's poroelastic losses. Only for the reusable face masks (**B**) this approach ($n = 0.5$) shows a very poor fitting. In this case, the n factor is allowed to change to find the best fitting (solid line, **B**). The parameters obtained from the fitting of phase and magnitude spectra are in Table 2.

measurements. The obtained results are similar as for the whole face mask, with a strong dispersive response below 400 kHz and an asymptotic response for higher frequencies (see Fig. S2). Then, magnitude spectra measurements are used, as before, to obtain ϕ and α_0, and n (Eqs. 6 and 9). In this case we tried to keep $n = 0.5$ unless fitting was not possible (as observed with woven face mask in previous section). In this case, it is only necessary to consider $n > 0.5$ for the additional filter layers. Results are collected in Table 2. First and last layers cannot be described by this approach, probably loss is too low and material too inhomogeneous to be reproduced by Eq. (7).

3.2.3. *Comparison of whole facemask results with individual layers*

The purpose of this comparison is to get some further insight into the propagation of the ultrasound wave through the face masks. There are two possibilities: i) the ultrasound wave goes from one layer to the next passing through a thin air–gap between the layers (loose layers condition) or ii) the ultrasonic wave pass from one layer directly to the next (well bounded layers condition). In both cases the phase shift for the whole facemask and the phase shift obtained by adding the contribution of all layers must be the same. Quite on the contrary, the loss for the whole face mask must be smaller if the wave is able to pass directly from one layer to the next as in this case reflection losses at the air/layer interfaces are avoided. If the wave has to cross the air–gap between layers, then the loss measured for the whole facemask and the loss obtained by adding the loss measured for each individual layer must be similar.

Main result obtained from this comparison (see data in Fig. 1 and Fig. 2, also Table S1 to make easier this comparison) is that both phase shift and magnitude loss are similar (for the whole face masks and the addition of individual layers). Therefore, from the ultrasonic point of view, the layer components of the facemask behave as loose layers. This is an expected result as the separation of the component layers of the facemask for the measurements revealed no bounding between them.

3.3. *Narrowband ultrasonic measurements*

Narrowband ultrasonic measurements were also performed. This technique presents the advantage of being simpler and cheaper to implement. The transmitter transducer can be driven by a conventional and general purpose low voltage (<20 V, peak to peak) function generator, the use of a preamplifier in reception can be avoided and there is no need of spectral analysis. The main drawback is that measurements are obtained at one single frequency, however, variation in the face mask response with the frequency can be analyzed by a discrete set of measurements as presented here. The purpose of these measurements is twofold. First, to determine the feasibility of these measurements. Second, to verify the equivalence of both techniques (narrowband and wideband). Three frequencies were selected for these

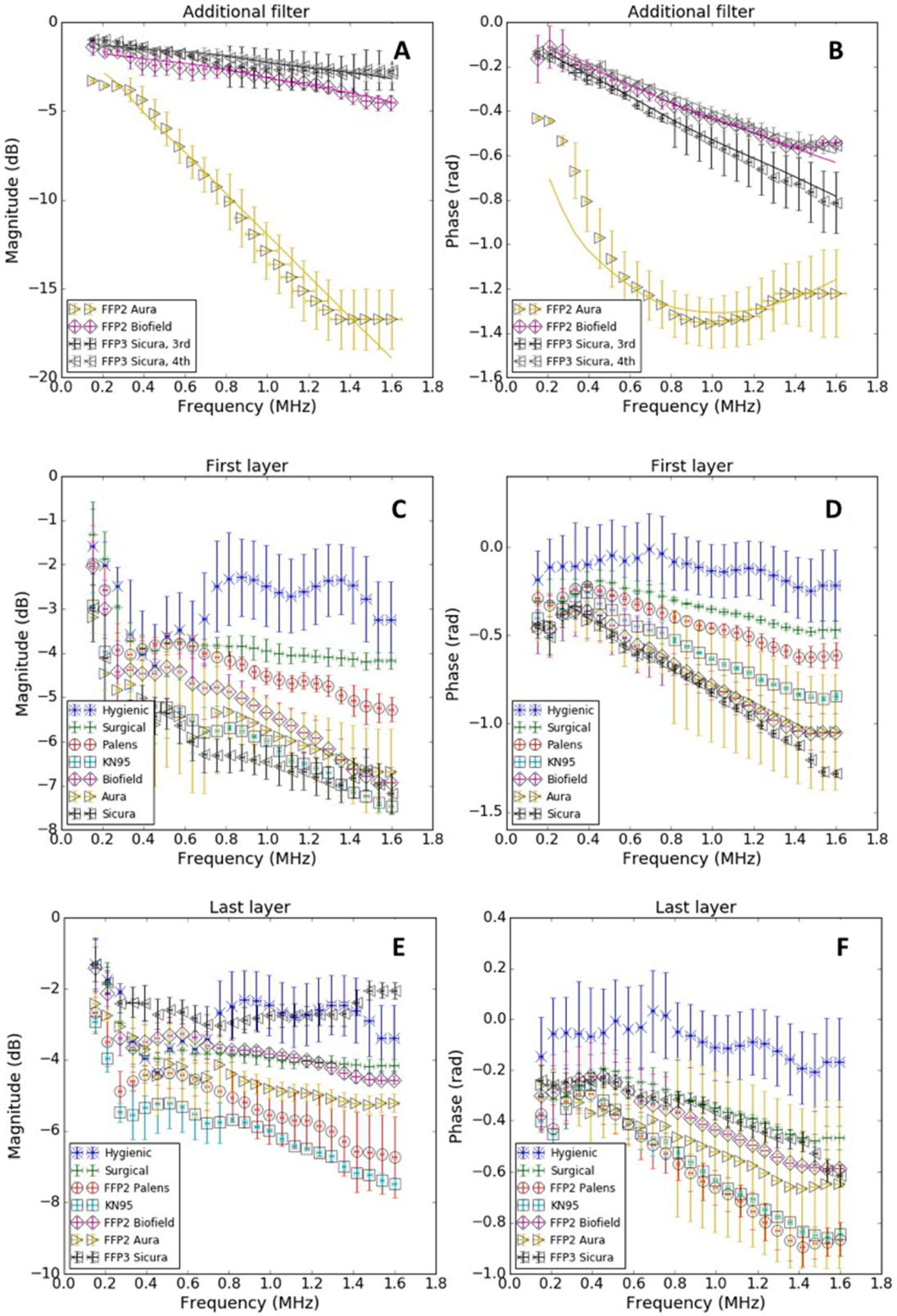

Fig. 3. Air-coupled ultrasonic transmission coefficient spectra for other component layers of the face masks: (**A**) magnitude of additional layer, (**C**) first layer and (**E**) last layer; (**B**) phase of additional layer, (**D**) first layer and (**F**) last layer. Markers correspond to the experimental data; Solid lines in **A** and **B** correspond to the calculated transmission coefficient using Eqs. (1), 2, 6, and 7, allowing parameter n (Eq. (7)) to be changed for the fitting. The parameters obtained from the fitting of phase and magnitude spectra are in Table 2. Additional filter layer (only for FFP2 Aura and Biofield and FFP3 Sicura): **A** and **B**. First layer (outer layer located outwards): **C** and **D**, Last layer (outer layer located next to the mouth): **E** and **F.**

measurements: 0.3, 0.7 and 1.4 MHz.

As an example, Fig. 4 shows the received signal (15 cycles tone burst) at 0.3, 0.7 and 1.4 MHz with and without the FFP3 Sicura face mask in between the transducers. Signals are normalized to facilitate the visualization. Similar results were obtained for the rest of the face masks. Phase delay is clearly observed as well as the decrease of the SNR due to the attenuation of the ultrasonic wave in the face mask. Table 4 summarized the amplitude loss and the phase shift measured for all face-masks with this technique at 0.3, 0.7 and 1.4 MHz. The comparison of these values with measurements in Fig. 1 show that both techniques (narrowband and wideband) provide similar results.

3.4. Microscopic images

Fig. 5 shows the obtained images of the filter layers of the face masks. The appearance of the main filter layer is similar in all cases, with the main exception of the FFP2 Palens filter layer that appears more porous. Although the appearance of the filter layer in hygienic and surgical face masks looks similar to the rest of FFP2, KN95 and FFP3 filter layers, it must be underlined the fact that the light intensity was larger in the former cases (for example Abbe condenser aperture is x20 for hygienic face mask filter and x48 for FFP2 Biofield filter layer, where a larger aperture of the Abbe condenser means a larger intensity of light). This can be due simply to the fact that filter layers of hygienic and surgical face masks are thinner (with the main exception of FFP3 Sicura filter layer that presents a similar thickness), however, other features that contribute to modify the amount of light transmitted through the face masks layers are the porosity or the pore size and tortuosity. In all cases, the additional filter layer (when present) presents a relatively higher porosity and larger pore size.

Fig. 6 shows the obtained images of the outer membranes of the face mask. The light transparency of all these layers is similar (in all cases Abbe condenser aperture is set to x4, which is the minimum amount of light intensity allowed) and much larger compared with filter layers in Fig. 5. Also the structure is similar with the main exceptions of the last layer of FFP2 Aura and FFP3 Sicura. Porosity seems to be larger for outer layers of hygienic face masks and for the last layer of the FFP2 Biofield and FFP3 Sicura.

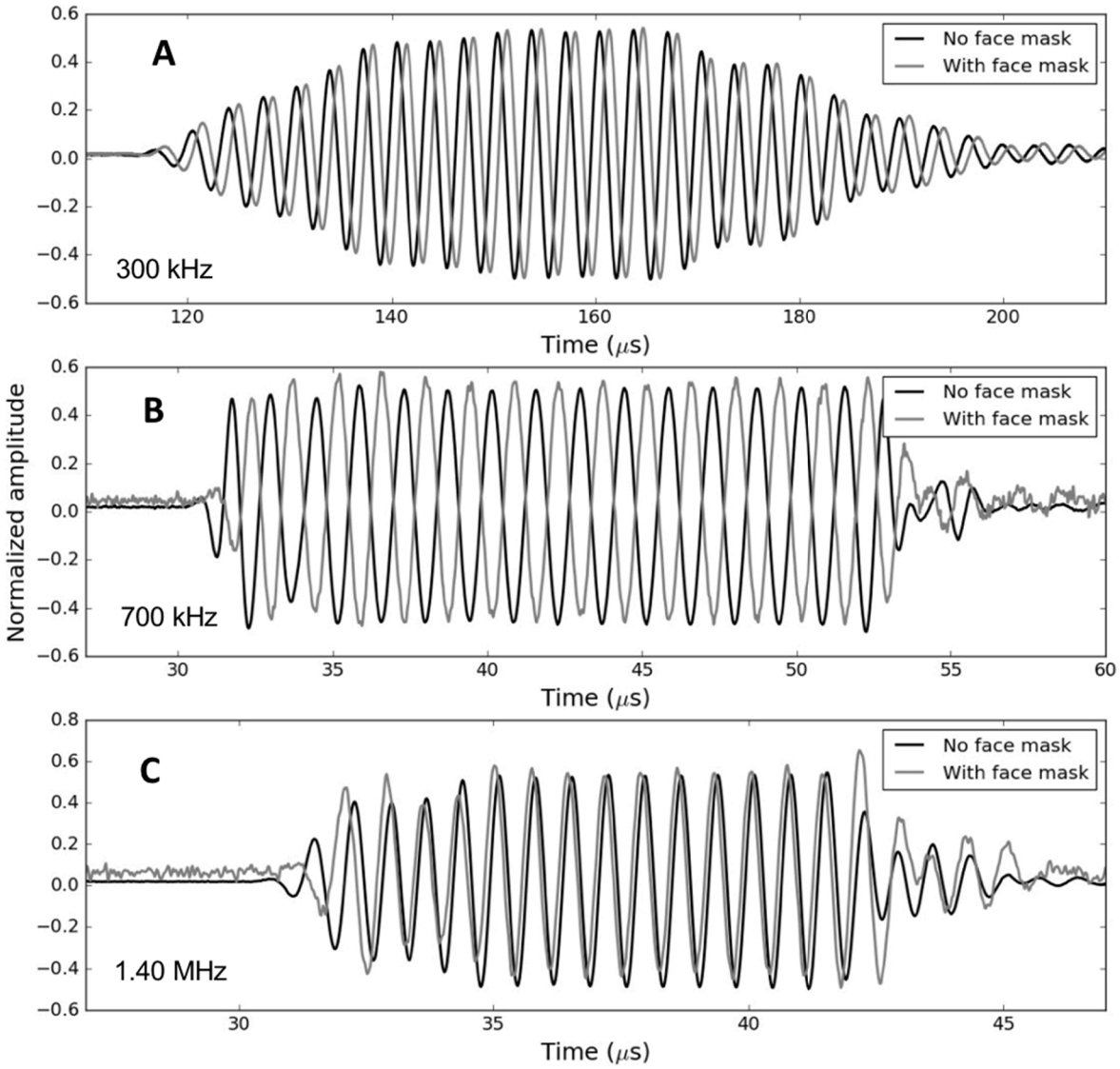

Fig. 4. Temporal normalized responses of narrowband ultrasonic tone burst excitation (15 cycle, 20 V peak to peak) through FFP3 Sicura face masks: (**A**) at 300 kHz; (**B**) at 700 kHz; and (**C**) at 1.4 MHz. Black line: signal received without the face mask between the transducers. Gray line: signal received with the face mask between the transducers. Normalization is performed to facilitate visualization of both signals; amplitude loss is presented in Table 3. Phase shift and reduction in SNR can be appreciated; tone burst received with the face mask between the transducers is delayed respect to the signal received without the face mask between the transducers is due to the lower velocity of ultrasound propagation in the face mask compared with the velocity in the free air.

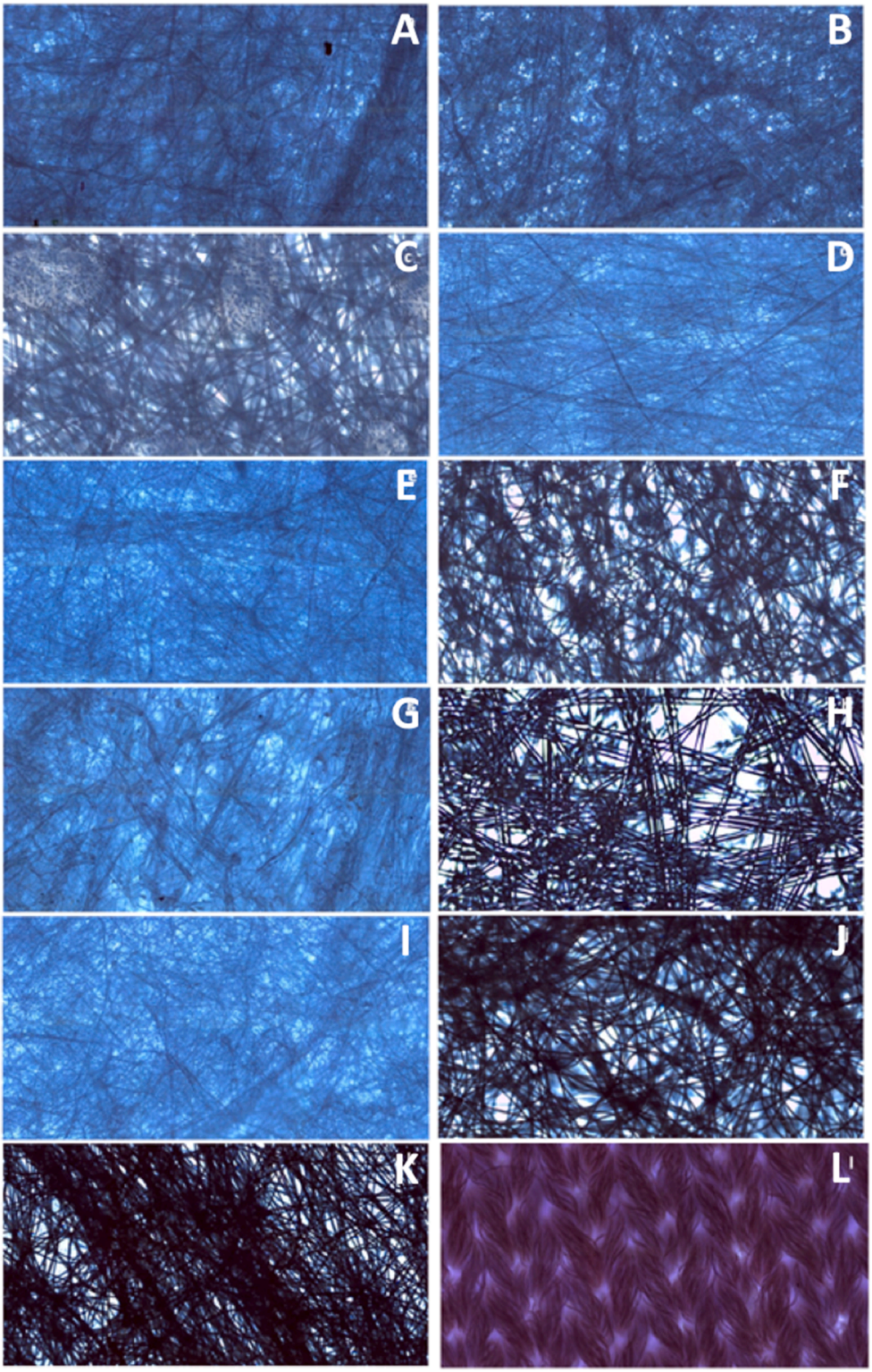

Fig. 5. Microscopic images of facemasks filters: in all cases magnification is x10. Abbe condenser aperture is indicated parenthetically. (**A**) Hygienic (x20), (**B**): Surgical (x22), (**C**): FFP2 Palens (x20), (**D**): KN95 (x35), (**E**): Biofield, paper like (x48), (**F**): Biofield, non-woven fibers (x11), (**G**): FFP2 Aura main filter (x48), (**H**): FFP2 Aura, translucent rigid fiber plate (x10), (**I**): FFP3, paper like layer (x36), (**J**): FFP3, non-woven fibers layer (x5), (**K**): FFP3 non-woven fibers layer (x5). (**I**): Fabric (x41).

4. Discussion

Measurements shown in Figs. 1- 4 and Table 4 demonstrate that it is possible to transmit ultrasonic waves in the frequency range 0.15–1.6 MHz both through face masks and through their layer components using a completely non-invasive and non-destructive technique based on air-coupled ultrasound. This can be realized using conventional ultrasonic equipment (pulser/receiver electronics) and specially developed air-coupled transducers. Alternatively, this can also be done by using tone burst excitation. In this case, a conventional low voltage function generator can be used, no spectral analysis is necessary and no gain in reception is required. Results from both techniques are coincident (within the observed variability of the measurements), see Table 4 and Fig. 1.

A key result of this work is that each face mask type presents a distinctive ultrasonic signature. Out of the 9 different types of face

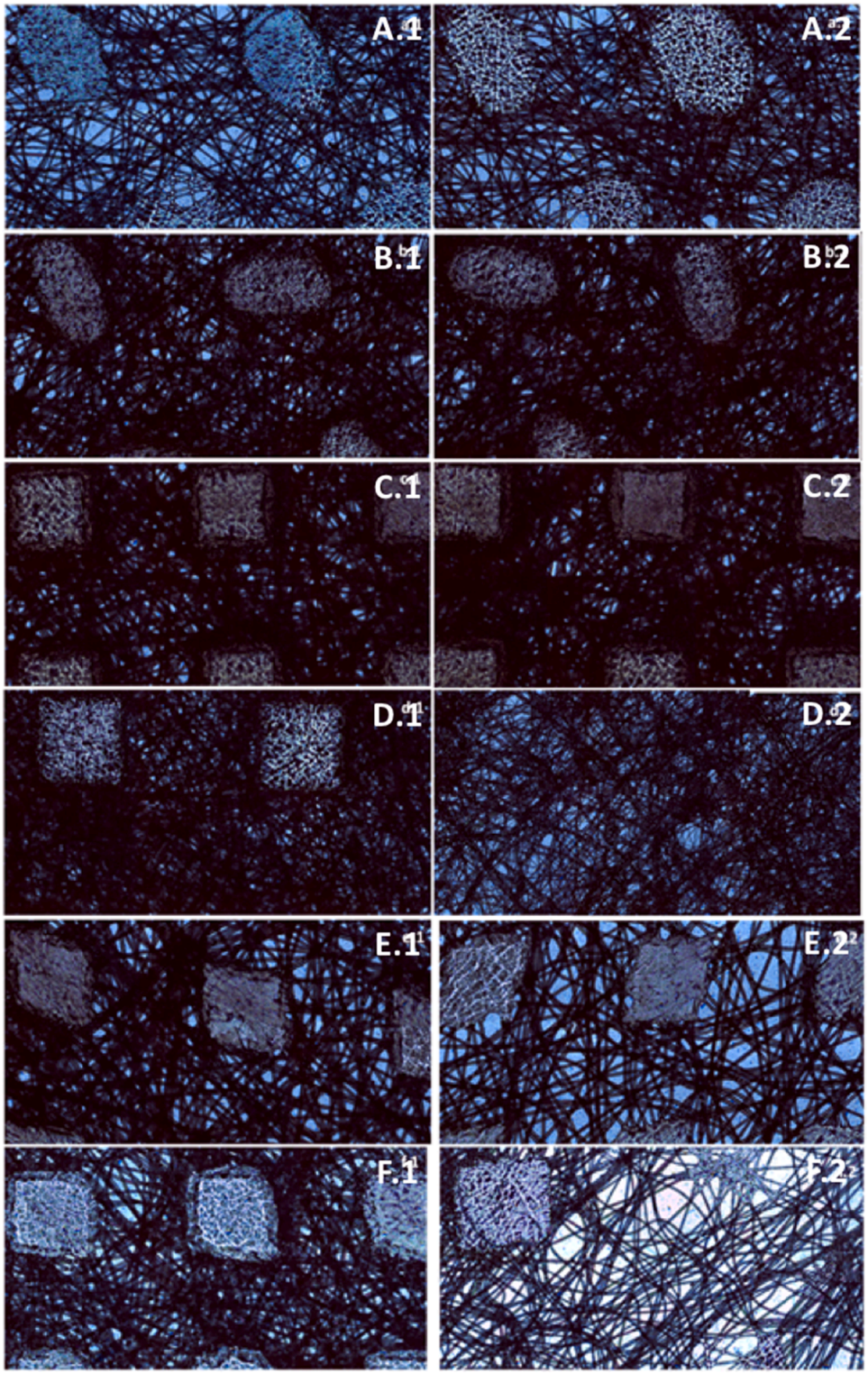

Fig. 6. Microscopic images of outer layers: in all cases magnification is x10 and Abbe condenser aperture is x4. Index 1: first layer (outwards), index 2: last layer (inwards, closer to the mouth). (**A**) Surgical, (**B**): FFP2 Palens, (**C**): KN95 PinzTech, (**D**): FFP2 Aura, (**E**): FFP2 Biofield, (**F**): FFP3 Sicura.

masks tested, only two of them presented a similar response (with differences within experimental variability): FFP3 Sicura and KN95 PinzTech. This ultrasonic signature can be obtained by the measurement of the transmission coefficient spectra either by using a wideband technique (magnitude and phase, see Fig. 1), or, alternatively, by using narrowband measurements at a discrete set of frequencies (for instance, our proposal in this work was to use: 0.3, 0.7 and 1.4 MHz, see Table 4). Once this ultrasonic signature of a given face mask type is known, it can be used to verify if a face mask sample of a given type meets the expected response. As this measurement is very fast, completely non-invasive and non-destructive, rather cheap, suitable for operation in industrial environments and to be adapted for continuous testing, this can be applied as an in-line quality control test in face mask fabrication. Alternatively, this can be used to assess or to monitor face mask properties alteration due to

their usage or due to the exposure to different environmental conditions (temperature, aerosols, dust, etc…) or due to the application of disinfection methods, etc.

Another result of this work is that the ultrasonic technique can also contribute to study filtration efficiency or breathability of the face masks, when used in conjunction with other techniques. Being an indirect measurement, the main value of the technique is given by the properties mentioned above (non-destructive, non-invasive, fast, cheap, and suitable for industrial environments). For the purpose of the study of the face masks filtration efficiency and breathability, it is very interesting the fact that the observed ultrasonic propagation in the face masks takes place through the air in the pores of the face masks. Therefore, ultrasonic parameters like velocity of propagation, attenuation coefficient and variation of these two parameters with the frequency will be affected by face mask properties like: pore size, pore tortuosity and sinuosity, porosity, permeability, etc., that are also closely related with filtration efficiency and breathability.

A first ultrasonic criterion for face mask efficiency can be based on the variation of the losses in the attenuation coefficient with the frequency, where it can be imposed that it must follow the behavior given by $\alpha \propto f^n$, with $n = 0.5$. The reason for this is that this corresponds to the attenuation predicted by low-frequency Biot's theory where attenuation is determined by the viscous interaction between the fluid in the pores and the solid as the pore size is smaller than the viscous skin depth. In addition, this is the case of all hygienic, surgical, KN95, FFP2 and FFP3 face masks studied. However, woven reusable face masks present a value on n clearly larger and close to 0.7. This is not a good indicator of filtration efficiency as this indicates that in these face masks pores are larger and the viscous interaction between the air and the solid is not so strong.

After checking that behavior of the attenuation coefficient with the frequency follows a $\alpha \propto f^{0.5}$ law another ultrasonic criterion can be based on the value of the transmission coefficient magnitude and phase spectra. As phase can be more difficult to measure in an industrial environment, we can limit this analysis to magnitude loss. For a given frequency, for example 0.7 MHz, the observed loss is about −16 dB for hygienic face masks, about −20 dB for surgical face masks, about −28 dB for KN95 (only one type of face mask measured: PinzTech) and in the range –23 to −39 dB for FFP2 and FFP3 (only one type of FFP3 measured: Sicura). Further studies in this direction could contribute to determine if such classification is feasible and its potential interest.

On the other hand, the loss in the ultrasonic transmission coefficient magnitude can also be related to the breathability of the face mask, as the larger the friction between the air and the solid in the pores of the face mask, the larger the pressure drop across the face mask. This feature is normally characterized by measuring the Maximum Breathing Resistance (MBR) for exhalation (at 30 and 95 l/min) and inhalation (at 160 l/min). These data are only available from manufacturers of face masks FFP2 Palens and Aura. Filtration efficiency can be expected to be similar in both cases (both face mask types are rated as FFP2) however there are significant differences in the MBR, which is larger in the case of the FFP2 Aura face mask (see Table 1). In view of the MBR data, it can be expected a larger loss of the ultrasonic transmission coefficient magnitude for the FFP2 Aura face mask. This is confirmed by measurements in Fig. 1 and Table 4. For example, at 0.7 MHz, magnitude loss of the ultrasonic transmission coefficient is −38 dB and –23 dB for FFP2 Aura and FFP2 Palens, respectively. A huge difference of 15 dB.

Finally, it can be observed in Fig. 1 that the response of FFP3 Sicura and KN95 PinzTech is very similar (magnitude loss at 0.7 MHz is about −28 dB in both cases). As in this case filtration efficiency is expected to be better for the FFP3 Sicura face mask, it could be anticipated, in view of the ultrasonic results, that breathability of the FFP3 Sicura face mask is also better. However, this cannot be confirmed as no data are available.

It is clear that filtration efficiency and breathability as well as ultrasonic transmission coefficient depend on both materials properties and face mask thickness (and number of layers). So far, we have analyzed ultrasonic properties that depend on both features (material parameters and thickness), like magnitude loss and phase shift. On the other hand, the dependency of the attenuation coefficient and the velocity with the frequency are material parameters and do not depend on the thickness of the face masks. The analysis of these material parameters can provide some further insight into the material filtration efficiency. In addition to n, it is also possible to obtain v_0 and m (Eq. (8)), α_0 (Eq. 9) and ϕ (Eq. (6)). v_0 is related to pore tortuosity, α_0 to pore size and permeability and ϕ to the ratio of open (air) to solid surface at the face mask / air interface. Therefore all these parameters can be expected to be related to both filtration efficiency and breathability.

The obtained value of α_0 (see Table 3) for KN95, FFP2 and FFP3 face masks is around 2200 Np/m (for $f_0 = 1$ MHz), while it is larger for hygienic and surgical face masks (3300 and 4700 Np/m, respectively), which suggest that the better filtration efficiency of the former face masks is not obtained by smaller pores (higher ultrasonic attenuation coefficient) but by thicker filters and the use of additional layers. This strategy of combining several filter layers can contribute to better filtration efficiency together with better breathability.

Obtained surface porosity for the non-reusable whole face masks varies from 0.41 to 0.85, while for reusable face masks it is about 0.85. No clear relationship between face mask grade and surface porosity has been observed.

The ultrasound velocity at 1.6 MHz seems to be close to the high frequency limit (see Figs. 1 and 2 and Fig S2). This value is closely related to the pore tortuosity (Eq. (3)). The more tortuous the pores, the more likely a particle (or droplet) will interact with the solid part of the filter and the more likely it can be trapped. In addition, the more tortuous the pores the larger pressure drop across the membrane. Ultrasound velocity at 1.6 MHz (obtained from Figs. 1 and 2) together with the estimated tortuosity value are listed in Table S4. Tortuosity values for the whole face masks varies from 1.28 (FFP3 Sicura) up to 1.59 (Hygienic), while for the main filter varies from 1.40 (FFP2 Palens) up to 2.41 (FFP3 Sicura). It seems that the face mask with a lower filtration efficiency (hygienic) present a larger tortuosity, hence, the better filtration efficiency of the other face masks must be provided by either the larger thickness or the use of more layers or both.

The measurements of the response of the individual layer components of the face masks (Figs. 2 and 3) reveal some interesting features. In the first place, it can be observed that the magnitude loss and phase shift measured in the whole face masks can be obtained as the addition of the measured response of the individual component layers, this means that attenuation coefficient calculation presented before not only depend on the ultrasonic loss in the layers, but also to the losses produced in the layers interfaces. These measurements also reveal that the main contribution to the face mask transmission coefficient loss and phase shift is due to the main filter layer in the face mask, as it was expected.

These layers also present a variation in the attenuation coefficient governed by a power law with exponent equal to 0.5. Some face masks present an additional filter layer which is thinner (apart from FFP2 Biofield) and presents larger pores (see Fig. 5). In these layers $\alpha \propto f^n$, with n between 1 and 1.4, revealing the fact that the presence of bigger pores in these cases reduces the contribution of the low-frequency poroelastic losses, and hence increases the value of n.

There is also a clear difference between ultrasonic responses of the filter layers of the different face masks (see Fig. 2). Let's take 0.7 MHz as the reference frequency for this analysis. As observed before, the lower magnitude loss and phase shift in the transmission coefficient correspond to the filter layers in hygienic and surgical face masks is about (-9 and −11 dB and −0.7 rad, respectively). These layers are also the ones that required the lowest light intensity to obtain the microscopic images (see Fig. 5, with Abbe condenser aperture set to x20 and x22, respectively). The largest losses and phase shift correspond to the filter layers of FFP2 Aura and FFP2 Biofield (-21 and −19 dB; and −1.7 and −2.0

rad, respectively). These layers are also the ones that required the largest light intensity to obtain the microscopic images (see Fig. 5, with Abbe condenser aperture set to x48).

In spite of this rather similar response of FFP2 Aura and FFP2 Biofield, it is remarkable the differences in the filter layer thicknesses. The filter layer in the FFP2 Aura face mask is 490 ± 20 μm, while the filter layer of the FFP2 Biofield is much thinner 190 ± 20 μm. The fact that the magnitude loss in the transmission coefficient is similar is explained by the fact that α_0 is much larger for the FFP2 Biofield filter (11400 Np/m) than for the FFP2 Aura filter (3200 Np/m), also the tortuosity is larger for the FFP2 Biofield. These two face masks present an additional filter layer, with an inverse strategy: low attenuation coefficient for the FFP2 Biofield and a larger attenuation coefficient for the FFP2 Aura. These features reveal two different strategies that can achieve a similar filtration efficiency (both face masks are rated as FFP2). A similar reasoning can be applied in the comparison between hygienic and surgical face masks, as thickness of the filter layers is similar for both cases, the better grading of the surgical face masks can be explained by the larger attenuation coefficient and the larger tortuosity measured in the later.

Another interesting result is obtained from the comparison of the spectra of the main filter in the FFP3 Sicura and the KN95 PinzTech face masks. Both filters present similar magnitude loss response, though the filter layer of the FFP3 Sicura layer is thinner. This is the result of a larger attenuation coefficient of the material in the FFP3 Sicura filter layer (Table 3). Another difference is the tortuosity, larger for the FFP3 Sicura main filter (Table S4).

5. Conclusions

This work shows that it is possible to measure the ultrasonic transmission coefficient in the frequency range 0.15–1.6 MHz in different types of face masks (from hygienic to FFP3, reusable and non-reusable) and their component layers using an ultrasonic air-coupled technique. Two different versions of the ultrasonic technique have been presented and tested, one using wideband pulses and the other using narrowband tone bursts with equivalent results. The former can provide more information while the later can be implemented in an easier way. Results show that there are remarkably large variations in the ultrasonic response of face masks of different types.

Measurement of the ultrasound velocity and the attenuation coefficient in the face masks and the variation in these parameters with the frequency permitted to determine that the propagation of the ultrasonic wave through the face masks takes place through the pore space. The propagation of the ultrasonic wave through the face mask (both velocity and attenuation) is then affected by face mask features like porosity, pore size, pore tortuosity, permeability, etc. Moreover, results point out the fact the dominant effect in the attenuation of the wave is due to the viscous drag between the air and the fibers (which depends on the relationship between the pore size and the wavelength), while velocity is also affected by the tortuosity of the pores. That is, the ultrasonic technique is an indirect way to measure face mask properties that are related with the filtration efficiency and the breathability. The results also show that the measured ultrasonic transmission coefficient is also affected by face mask thickness, number of layers, density and surface porosity.

Measurements reveal that there are large differences in the transmission coefficients measured in face masks of different types, and that each face mask type presents a particular ultrasonic signature that can be used to characterize them or to verify the face mask integrity.

This is quite convenient as this is a completely non-invasive, non-destructive and fast technique that can be easily implemented at an industrial scale for the in-line test of the production. In addition, these measurements have an indirect character and must be related with actual filtration properties, in this sense the technique can be very useful when combined with other direct techniques that may be more complex or time consuming or expensive or that are destructive. Alternatively, the technique is also well adapted to detect face masks modifications in an easy, fast and cheap way, for example during use, or after disinfection or after being exposed to different environments.

This work shows the viability to measure face mask and layer components using air-coupled ultrasound and suggests the interest and possibilities of this technique for quality control in this industry. Future work must contemplate the analysis of the quantitative correlation between filtration and breathability with ultrasonic parameters and the determination of the sensitivity of the ultrasonic parameters to the variation of the former parameters. For implementation in the industry, it will be necessary to determine, for a given model, the tolerance in filtration efficiency and breathability and how these tolerances translates into the ultrasonic parameters so that the ultrasonic method can be used to classify the production and to reject those cases that are beyond tolerance.

Competing interests: Authors declare that they have no competing interests.

Data and materials availability: All data are available in the main text or the supplementary materials.

CRediT authorship contribution statement

Tomás E. Gómez Álvarez-Arenas: Conceptualization, Methodology, Visualization, Supervision, Writing – original draft, Writing – review & editing, Measurements, Data analysis. **María D. Fariñas:** Visualization, Writing – original draft, Writing – review & editing, Data analysis. **Alba Ginel:** Measurements, Writing – review & editing.

Declaration of Competing Interest

The authors declare that they have no known competing financial interests or personal relationships that could have appeared to influence the work reported in this paper.

Acknowledgments

Funding: This work was supported by:

Spanish Agency of Science Technology and Research grant RTC-2017-6314-2 (TGAA, AG).

Spanish Ministry of Science grant FJCI-2017-34759 (MDF).

Face masks icons in graphical abstract made by freepik : [https://www.flaticon.com/authors/freepik]. Authors also acknowledge the assistance of VATC - CSIC for the protection of related IP rights.

Appendix A. Supplementary material

Supplementary data to this article can be found online at https://doi.org/10.1016/j.ultras.2021.106556.

References

[1] C.J. Worby, H.-H. Chang, Face mask use in the general population and optimal resource allocation during the COVID-19 pandemic, Nat. Commun. 11 (2020) 4049, https://doi.org/10.1038/s41467-020-17922-x.

[2] R. Mittal, R. Ni, J.-H. Seo, The flow physics of COVID-19, J. Fluid Mech. 894 (2020) F2, https://doi.org/10.1017/jfm.2020.330.

[3] J. Howard, A. Huang, Z. Li, Z. Tufekci, V. Zdimal, H.-M. van der Westhuizen, A. von Delft, A. Price, L. Fridman, L.-H. Tang, V. Tang, G.L. Watson, C.E. Bax, R. Shaikh, F. Questier, D. Hernandez, L.F. Chu, C.M. Ramirez, A.W. Rimoin, An evidence review of face masks against COVID-19, Proc. Natl. Acad. Sci. 118 (2021), e2014564118, https://doi.org/10.1073/pnas.2014564118.

[4] CDC, CDC on Homemade Masks, (2020). https://www.cdc.gov/coronavirus/2019-ncov/prevent-getting-sick/how-to-make-cloth-face-covering.html (accessed February 9, 2021).

[5] E.-D.-G. for H. and F. Safety, Guidance on regulatory requirements for medical face masks: Options for supporting production and/or placing on the market of medical face masks in the context of COVID-19 pandemic, Brussels (Belgium), 2020. https://www.ecdc.europa.eu/en/publications-data/using-face-masks-community-reducing-covid-19-.

[6] D. Lepelletier, B. Grandbastien, S. Romano-Bertrand, S. Aho, C. Chidiac, J.-F. Géhanno, F. Chauvin, What face mask for what use in the context of the COVID-19 pandemic? The French guidelines, J. Hosp. Infect. 105 (3) (2020) 414–418, https://doi.org/10.1016/j.jhin.2020.04.036.
[7] C. Matuschek, F. Moll, H. Fangerau, J.C. Fischer, K. Zänker, M. van Griensven, M. Schneider, D. Kindgen-Milles, W.T. Knoefel, A. Lichtenberg, B. Tamaskovics, F. J. Djiepmo-Njanang, W. Budach, S. Corradini, D. Häussinger, T. Feldt, B. Jensen, R. Pelka, K. Orth, M. Peiper, O. Grebe, K. Maas, P.A. Gerber, A. Pedoto, E. Bölke, J. Haussmann, Face masks: benefits and risks during the COVID-19 crisis, Eur. J. Med. Res. 25 (2020) 32, https://doi.org/10.1186/s40001-020-00430-5.
[8] Dana Mackenzie, Reuse of N95 Masks, Engineering. 6 (6) (2020) 593–596, https://doi.org/10.1016/j.eng.2020.04.003.
[9] L. Pirker, A. Pogačnik Krajnc, J. Malec, V. Radulović, A. Gradišek, A. Jelen, M. Remškar, I. B. Mekjavić, J. Kovač, M. Mozetič, L. Snoj, Sterilization of polypropylene membranes of facepiece respirators by ionizing radiation, J. Membr. Sci.,Vol. 619, 2021, 118756, 10.1016/j.memsci.2020.118756.
[10] S.-A. Lee, D.-C. Hwang, H.-Y. Li, C.-F. Tsai, C.-W. Chen, J.-K. Chen, Particle Size-Selective Assessment of Protection of European Standard FFP Respirators and Surgical Masks against Particles-Tested with Human Subjects, J. Healthc. Eng. 2016 (2016) 1–12, https://doi.org/10.1155/2016/8572493.
[11] M, Comparison of FFP2 , KN95 , and N95 and Other Filtering Facepiece Respirator Classes M Personal Safety Division, (2020) 2–4.
[12] M.H. Chua, W. Cheng, S.S. Goh, J. Kong, B. Li, J.Y.C. Lim, L. Mao, S. Wang, K. Xue, L. Yang, E. Ye, K. Zhang, W.C.D. Cheong, B.H. Tan, Z. Li, B.H. Tan, X.J. Loh, Face Masks in the New COVID-19 Normal: Materials, Testing, and Perspectives, Research. 2020 (2020) 1–40. 10.34133/2020/7286735.
[13] Norbert Serfozo, Jakub Ondráček, Naděžda Zíková, Mihalis Lazaridis, Vladimír Ždímal, Size-Resolved Penetration of Filtering Materials from CE-Marked Filtering Facepiece Respirators, Aerosol Air Qual. Res. 17 (5) (2017) 1305–1315, https://doi.org/10.4209/aaqr.2016.09.0390.
[14] E.P. Fischer, M.C. Fischer, D. Grass, I. Henrion, W.S. Warren, E. Westman, Low-cost measurement of face mask efficacy for filtering expelled droplets during speech, Sci. Adv. 6 (2020) eabd3083, https://doi.org/10.1126/sciadv.abd3083.
[15] Kajanan Selvaranjan, Satheeskumar Navaratnam, Pathmanathan Rajeev, Nishanthan Ravintherakumaran, Environmental challenges induced by extensive use of face masks during COVID-19: A review and potential solutions, Environ. Challenges. 3 (2021) 100039, https://doi.org/10.1016/j.envc.2021.100039.
[16] J. Van Loon, L. Veelaert, S. Van Goethem, R. Watts, S. Verwulgen, J.C. Verlinden, E. Du Bois, Reuse of Filtering Facepiece Respirators in the COVID-19 Era, Sustainability. 13 (2021) 797, https://doi.org/10.3390/su13020797.
[17] W. Kools, S. Konagurthu, A.R. Greenberg, L.J. Bond, W.B. Krantz, T.H. van den Boomgaard, H. Strathmann, Use of acoustic time-domain reflectometry for real-time measurement of thick-ness changes during evaporative casting of polymeric films, J. Appl. Polym. Sci. 69 (1998) 2013–2019.
[18] J. Li, R.D. Sanderson, E.P. Jacobs, Non-invasive visualization of the fouling of microfiltration membranes by ultrasonic time-domain reflectometry, J. Memb. Sci. (2002), https://doi.org/10.1016/S0376-7388(01)00664-0.
[19] T.E.G. Álvarez-Arenas, Air-coupled ultrasonic spectroscopy for the study of membrane filters, J. Memb. Sci. 213 (2003) 195–207. http://www.sciencedirect.com/science/article/pii/S0376738802005276.
[20] S. Ramaswamy, A.R. Greenberg, M.L. Peterson, Non-invasive measurement of membrane morphology via UFDR: pore-size characterization, Journal of Membrane Science 239 (1) (2004) 143–154, https://doi.org/10.1016/j.memsci.2003.08.030.
[21] T.E. Gómez Álvarez-Arenas, P.Yu. Apel, O.L. Orelovich, Characterization of ion-track membranes by non-contact ultrasonic magnitude and phase spectroscopy, J. Memb. Sci. 301 (1-2) (2007) 210–220, https://doi.org/10.1016/j.memsci.2007.06.024.
[22] M.A. Biot, Theory of Propagation of Elastic Waves in a Fluid-Saturated Porous Solid. I. Low-Frequency Range, J. Acoust. Soc. Am. 28 (1956) 168–178. 10.1121/1.1908239.
[23] M.A. Biot, Theory of Propagation of Elastic Waves in a Fluid-Saturated Porous Solid. II. Higher Frequency Range, J. Acoust. Soc. Am. 28 (1956) 179–191. 10.1121/1.1908241.
[24] K. Attenborough, The influence of microstructure on propagation in porous fibrous absorbents, J. Sound Vib. 16 (3) (1971) 419–442, https://doi.org/10.1016/0022-460X(71)90597-9.
[25] R.F. Lambert, J.S. Tesar, Acoustic structure and propagation in highly porous, layered, fibrous materials, J. Acoust. Soc. Am. 76 (1984) 1231–1237. 10.1121/1.391417.
[26] T.E. Gómez Alvarez-Arenas, L. Elvira Segura, E. Riera Franco de Sarabia, Generation of the slow wave to characterize air filled porous fabrics, J. Appl. Phys. 78 (1995) 2843–2845. 10.1063/1.360714.
[27] T.E.G. Alvarez-Arenas, A nondestructive integrity test for membrane filters based on air-coupled ultrasonic spectroscopy, IEEE Trans. Ultrason. Ferroelectr. Freq. Control. 50 (6) (2003) 676–685, https://doi.org/10.1109/TUFFC.2003.1209555.
[28] T.E. Gómez Álvarez-Arenas, B. González, P.Y. Apel, O.L. Orelovitch, A. V. Mitrofanov, Ultrasound propagation in the micropores of track membranes, Appl. Phys. Lett. 87 (2005), 111911, https://doi.org/10.1063/1.2045542.
[29] T.E.G. Alvarez-Arenas, P.Yu. Apel, O. Orelovitch, Ultrasound attenuation in cylindrical micro-pores: Nondestructive porometry of ion-track membranes, IEEE Trans. Ultrason. Ferroelectr. Freq. Control. 55 (11) (2008) 2442–2449, https://doi.org/10.1109/TUFFC.951.
[30] T.E. Gomez Alvarez-Arenas, Acoustic impedance matching of piezoelectric transducers to the air, IEEE Trans. Ultrason. Ferroelectr. Freq. Control. 51 (5) (2004) 624–633, https://doi.org/10.1109/TUFFC.2004.1308697.
[31] T. Gómez Álvarez-Arenas, E. Gil-Pelegrin, J. Ealo Cuello, M. Fariñas, D. Sancho-Knapik, D. Collazos Burbano, J. Peguero-Pina, Ultrasonic Sensing of Plant Water Needs for Agriculture, Sensors. 16 (2016) 1089. 10.3390/s16071089.
[32] T.E. Gómez Álvarez-Arenas, P.Yu. Apel, O.L. Orelovitch, M. Muñoz, New ultrasonic technique for the study of the pore shape of track-etched pores in polymer films, Radiat. Meas. 44 (9-10) (2009) 1114–1118, https://doi.org/10.1016/j.radmeas.2009.09.002.
[33] Peter B. Nagy, Slow wave propagation in air-filled permeable solids, J. Acoust. Soc. Am. 93 (6) (1993) 3224–3234, https://doi.org/10.1121/1.405707.
[34] T.E.G. Álvarez-Arenas, S. De La Fuente, I. González Gómez, Simultaneous determination of apparent tortuosity and microstructure length scale and shape: Application to rigid open cell foams, Appl. Phys. Lett. 88 (2006), 221910, https://doi.org/10.1063/1.2208921.
[35] Wu Qunli, Empirical relations between acoustical properties and flow resistivity of porous plastic open-cell foam, Appl. Acoust. 25 (3) (1988) 141–148, https://doi.org/10.1016/0003-682X(88)90090-4.
[36] Tomás E. Gómez Álvarez-Arenas, Simultaneous determination of the ultrasound velocity and the thickness of solid plates from the analysis of thickness resonances using air-coupled ultrasound, Ultrasonics. 50 (2) (2010) 104–109, https://doi.org/10.1016/j.ultras.2009.09.009.
[37] H. Deresiewicz, T. Rice, The effect of boundaries on wave propagation in a liquid-filled porous solid: V. Transmission across a plane interface, Bull. Seismol. Soc. Am. 54 (1964) 409–416.
[38] L.M. Brekhovskikh, Waves in Layered Media, 2nd ed., Academic Press, inc., New York, 1980.
[39] Boris Gurevich, Michael Schoenberg, Interface conditions for Biot's equations of poroelasticity, J. Acoust. Soc. Am. 105 (5) (1999) 2585–2589, https://doi.org/10.1121/1.426874.